Applied Catalysis B: Environmental 125 (2012) 425–431

Contents lists available at SciVerse ScienceDirect

Applied Catalysis B: Environmental

journal homepage: www.elsevier.com/locate/apcatb

Microwave-assisted non-aqueous route to deposit well-dispersed ZnO nanocrystals on reduced graphene oxide sheets with improved photoactivity for the decolorization of dyes under visible light

Yu Liu [a], Yong Hu [a,*], Mojiao Zhou [a], Haisheng Qian [a], Xiao Hu [b]

[a] Key Laboratory of the Ministry of Education for Advanced Catalysis Materials, Institute of Physical Chemistry, Zhejiang Normal University, Jinhua, 321004, PR China
[b] School of Materials Science & Engineering, Nanyang Technological University, Singapore, 639798, Singapore

ARTICLE INFO

Article history:
Received 28 March 2012
Received in revised form 13 June 2012
Accepted 17 June 2012
Available online 26 June 2012

Keywords:
Reduced graphene oxide
ZnO nanocrystals
Nanohybrids
Microwave-assisted method
Photoactivity

ABSTRACT

A new strategy is discussed for deposition of monodisperse ZnO nanocrystals on the surface of reduced graphene oxide (rGO) sheets to form rGO/ZnO nanohybrids via a microwave-assisted route in a non-aqueous media. This is a facile and rapid process, which only requires a proration of zinc salt and rGO sheets react in diethylene glycol (DEG) under a low level of microwave irradiation (300 W) for 10 min. The as-prepared nanohybrids demonstrate well-dispersed ZnO nanocrystals loading and powerful photocatalytic activity for the decolorization of self-photosensitized dyes (rhodamine-B and methylene blue) under visible-light illumination. Here, DEG does not only help to enhance dispersion of rGO sheets, but also play an important role of controlling the growth of ZnO. Furthermore, the average size and loading amount of ZnO nanocrystals can be conveniently varied or controlled by the concentration of zinc precursor. The result uncovers that the loading of ZnO nanocrystals in the as-prepared nanohybrids is crucial to obtain an optimal synergistic effect between ZnO and rGO sheets in the mediated photocatalysis process for the photosensitized dyes decolorization. Accordingly, the optimum matching for the best photocatalytic activity is investigated thoroughly and a reasonable mechanism is also proposed.

1. Introduction

In the past few decades, high efficiency and stable photocatalytic materials have been extensively studied for the degradation of organic pollutes and developed their potential applications to environmental remediation [1]. Zinc oxide (ZnO), with a large band gap (3.37 eV), is one of the most popular photocatalysts due to its chemical stability, non-toxicity nature and high photocatalytic activity in the removal of pollutants in water or air [2–4]. However, the photo-corrosion of ZnO that occurs with the ultraviolet (UV) light irradiation, as well as the susceptibility of ZnO to facile dissolution at extreme pH values, have significantly decreased the photocatalytic activity of ZnO in aqueous solution and blocked the application of ZnO in photocatalysis [5]. Besides, ZnO can only absorb the UV light ($\lambda < 368$ nm), but solar spectrum consists of 5–7% of UV light, 46% of visible-light and 47% of infrared radiation [6,7]. Therefore, it is of great importance to improve the photocatalytic activity of ZnO using visible-light as the energy source for the degradation of the organic pollutants from the viewpoint of practical use and commercialization.

Very recently, many efforts have been exploited to enhance ZnO-based visible-light-active photocatalytic systems, such as doping ZnO with different metal ions and coupling of ZnO with narrow band gap semiconductor [8,9]. Another promising strategy to extend the photo-response of a semiconductor with a wide band gap to the visible region is to harvest visible-light by adsorbed dyes or other color species [10,11]. Moreover, it is well known that a high mobility for photoexcited electron–hole separation is very important to improve the catalytic performance of photocatalysts [12]. The conjugated materials have been proven to be a category of materials with unique properties in electron or hole transport, which can cause a rapid photoinduced charge separation and a relatively slow charge recombination in electron-transfer processes [13,14]. Many works have been devoted to reduce the recombination of charge carriers by coupling the photocatalysts with conjugative structure carbon materials, such as carbon nanotubes (CNTs) and graphite-like carbon [5,15,16]. Graphene is a perfect sp^2-hybridized two-dimensional material, composed of single-, bi- and few-layers of carbon atoms, forming six-membered rings with superior conductivity and larger surface area [17,18]. More importantly, the combination of semiconductors and graphene may be an ideal system to accelerate the charge transfer from photocatalyst to the liquid–solid interface contacting with organic pollutants by taking advantage of graphene's unique electron transport

* Corresponding author. Tel.: +86 579 82282234; fax: +86 579 82282595.
E-mail address: yonghu@zjnu.edu.cn (Y. Hu).

0926-3373/$ – see front matter © 2012 Elsevier B.V. All rights reserved.
http://dx.doi.org/10.1016/j.apcatb.2012.06.016

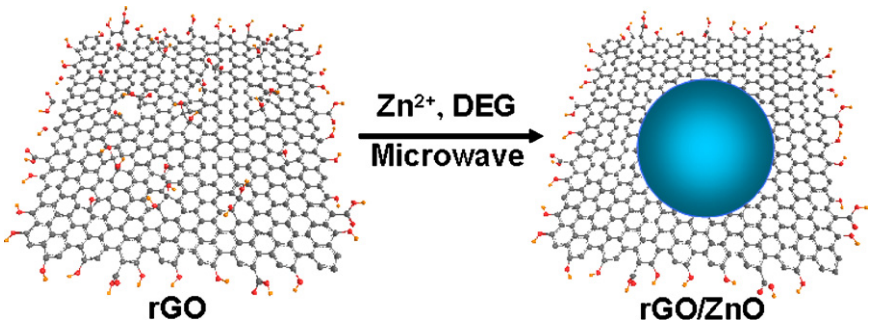

Scheme 1. Schematic illustration of the rGO/ZnO nanohybrids prepared via a rapid microwave-assisted method.

property [19,20]. Up to now, semiconductor nanocrystals such as TiO_2, ZnO and CdS have also been utilized to decorate graphene sheets to form graphene-supported nanomaterials with remarkable photocatalytic properties [21–23].

Microwave irradiation is an attractive and facile method for rapid synthesis of nanocrystals with small particle size, narrow particle size distribution, and high purity. Compared with conventional heating, it can promote nucleation and reduce the synthesis time considerably, generating smaller and more uniform particles [9,24–26]. Herein, we demonstrated a facile and rapid microwave-assisted irradiation method to directly deposit ZnO nanocrystals on the surface of reduced graphene oxide (rGO) sheets to form rGO/ZnO nanohybrids in diethylene glycol (DEG) media, and the principle of synthetic process is described in Scheme 1. This method shows the advantageous preparation of rGO/ZnO nanohybrids without employing catalysts, surfactants, complex metal ligands or fatty-acids to assist growth. Because only DEG and one kind of inorganic metal salt and rGO sheets are required, the products are of high purity and particularly suitable for catalysts. Furthermore, the average size and loading amount of ZnO nanocrystals anchored is conveniently controlled by varying the concentration of metal salt precursor. As expected, the as-prepared rGO/ZnO nanohybrids as an electron-transfer mediator exhibit excellent synergistic effect for the decolorization of rhodamine-B (RhB) and methylene blue (MB) dyes when exposed to visible-light irradiation. Accordingly, the optimum matching for the best photocatalytic activity was investigated thoroughly, and a reasonable mechanism was further proposed to explain the role of rGO sheets in rGO/ZnO nanohybrids.

2. Materials and methods

All reagents were analytical grade, purchased from the Shanghai Chemical Reagent Factory, and used as received without further purification.

2.1. Synthesis of rGO sheets via Fe reduction of graphene oxide (GO)

In a typical procedure, GO was prepared from pure graphite using a modified Hummer's method [27], and rGO sheets were obtained via Fe reduction of GO according to Fan's method [28]. Briefly, 2.0 g of natural graphite powder was added to 300 mL of H_2SO_4 under stirring at 0 °C, and then 3.0 g of $NaNO_3$ and 20 g of $KMnO_4$ were added sequentially. Successively, the mixture was transferred to a water bath at 30 °C and stirred for 20 min to form a thick paste. Then, 250 mL of distilled water was slowly added and the temperature was increased to 98 °C aging for 30 min. Additional 500 mL of water was added and followed by a slow addition of 40 mL of H_2O_2 (30%), turning the color of the solution from dark brown to brilliant yellow. The mixture was filtered and washed with diluted HCl aqueous (1/10 v/v) to remove metal ions, and then followed by washing with distilled water to remove the acid until the pH became 7.

To obtain rGO sheets, 0.5 g of Fe powder and 10 mL of HCl (37 wt%) were directly added into 50 mL of GO suspension at ambient temperature. The mixture was stirred for 30 min and then maintained for 6 h. After reduction, 10 mL of HCl (37 wt%) was added into the above solution in order to fully remove excess Fe powder. In the end, the resulting rGO sheets were collected by filtration, washed with distilled-water and ethanol several times, and dried at 80 °C for 8 h in a vacuum oven.

2.2. Synthesis of rGO/ZnO nanohybrids via a microwave-assisted method

In a typical procedure, 10 mg of as-prepared rGO sheets was added into a round-bottom flask and dissolved in 20 mL of DEG with the assistance of ultrasonication for 30 min. Successively, a certain amount of zinc acetate dihydrate ($Zn(AC)_2{\cdot}2H_2O$) was added into the above mixture under vigorous stirring for 30 min, and then were placed in a microwave refluxing system irradiated at 300 W for 10 min, resulting in rGO/ZnO nanohybrids. After collection by centrifugation, the final products were washed with ethanol for several times and dried at vacuum oven at 60 °C for 8 h. To investigate the effect of zinc salt on the formation of rGO/ZnO nanohybrids, the different concentration of zinc salt was used in the microwave process, while the other conditions remain unchanged. Products prepared with different amount of $Zn(AC)_2{\cdot}2H_2O$ (0, 0.0023, 0.0046, 0.0069, 0.0092 and 0.0115 M) after the microwave irradiation route were assigned sample codes as Sa (pure rGO sheets), Sb, Sc, Sd, Se and Sf, respectively (see Table 1).

2.3. Characterizations

The absorption spectra were measured using a PerkinElmer Lambda 900 UV–vis spectrophotometer at room temperature. Fourier transform infrared spectra (FT-IR) were recorded on a Nicolet NEXUS670 FT-IR spectrometer using KBr pellets. Powder X-ray diffraction (XRD) measurements of the samples were performed with a Philips PW3040/60 X-ray diffractometer using Cu

Table 1
The size and loading amount of ZnO nanocrystals in rGO/ZnO nanohybrids and the intensity ratios (I_D/I_G) for different samples.

Sample	Zn^{2+} concentration (M)	ZnO particle size (nm)[a]	ZnO loading (wt%)	I_D/I_G
Sa	0	–	0	1.91
Sb	0.0023	10.7	11.55	1.88
Sc	0.0046	11.2	16.49	1.48
Sd	0.0069	12.0	20.75	1.39
Se	0.0092	12.9	22.49	1.11
Sf	0.0115	13.8	26.89	0.92

[a] ZnO particle size was calculated from XRD diffraction data.

Kα radiation at a scanning rate of 0.06° s^{-1}. Scanning electron microscopy (SEM) was performed with a Hitachi S-4800 scanning electron micro-analyzer with an accelerating voltage of 15 kV. Transmission electron microscopy (TEM) and high-resolution transmission electron microscopy (HRTEM) were conducted at 200 kV with a JEM-2100F field emission TEM. Energy dispersive X-ray spectrometry (EDS) was performed with a spectroscope attached to HRTEM, which was used for elemental analysis. Samples for TEM measurements were prepared for TEM by dispersing the products in ethanol and placing several drops of the suspension on holey carbon films supported by copper grids. Raman spectra were collected by a Renishaw RM1000 confocal microprobe under ambient conditions, and the excitation wavelength was 514.5 nm. The photoluminescence spectra were recorded on an Edinburgh FLSP920 fluorescence spectrometer.

2.4. Photocatalytic activity of rGO/ZnO nanohybrids

The photocatalytic activities of the rGO/ZnO nanohybrids were evaluated by the decolorization of rhodamine-B (RhB) and methylene blue (MB) dyes (analytical grade) under visible-light illumination of a 500 W Xe lamp with a 420 nm cutoff filter. The reaction cell was placed in a sealed black box with the top opened, and the cutoff filter was placed to provide visible-light illumination. In a typical process, 12.5 mg of the as-prepared samples were added into 100 mL of RhB and MB solution (concentration: 10 mg/L), respectively. After being dispersed in an ultrasonic bath for 5 min, the mixture was stirred for 2 h in the dark to reach adsorption equilibrium between the catalyst and the solution. Then, the suspension was exposed to visible-light irradiation. The samples were collected by centrifugation at given time intervals to measure the absorption peak intensity of RhB (at 554 nm) and MB (at 665 nm) by using UV–vis spectroscopy.

•OH radical reactions were performed as follows. 2.5 mg of the different nanohybrids were suspended in 10 mL of RhB solution and 10 mL of aqueous solution containing 10 mM of NaOH and 5 mM of terephthalic acid (TA), respectively. Before exposure to visible-light, the suspension was stirred in the dark for 30 min. After irradiated for 10 min, the solutions were centrifuged for fluorescence spectroscopy measurements. A fluorescence spectrophotometer was used to measure the fluorescence signal of the 2-hydroxy-terephthalic acid (TAOH) generated. The excitation light wavelength used in recording fluorescence spectra was 320 nm.

3. Results and discussion

Because surface functional groups such as hydroxyl groups on rGO can act as favorable nucleation sites for guest materials, rGO become a competitive host substrate for the heterogeneous growth of desired active guest materials [29]. In this work, rapid deposition of ZnO nanocrystals on the surface of rGO sheets to form rGO/ZnO nanohybrids can be achieved in a microwave refluxing system at relatively low power of 300 W in DEG media. DEG does not only help to enhance dispersion of rGO sheets [30], but also play an important role of controlling the growth of ZnO [31,32]. The formation of high-quality ZnO nanocrystals was ascribed as the following equation [31]:

$$Zn(CH_3COO)_2 + xH_2O \xrightarrow{\Delta} Zn(OH^-)_x(CH_3COO^-)_{2-x} + xCH_3COOH \quad (1)$$

$$Zn(OH^-)_x(CH_3COO^-)_{2-x} \xrightarrow{\Delta} ZnO + (x-1)H_2O + (2-x)CH_3COOH \quad (2)$$

Eq. (1) is the hydrolysis reaction for $Zn(CH_3COO)_2$ to form metal complexes and the zinc complexes would dehydrate and remove acetic acid to form pure ZnO as Eq. (2) during the microwave irradiation process.

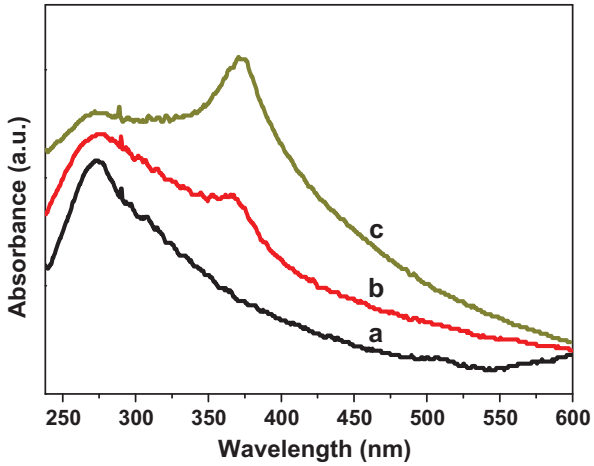

Fig. 1. UV–vis spectra of as-prepared (a) rGO sheets and rGO/ZnO nanohybrids with different concentration of Zn^{2+}: (b) 0.0023 M, (c) 0.0115 M.

Fig. 1 shows the UV–vis absorption spectra of the as-prepared rGO sheets and rGO/ZnO nanohybrids. From these spectra, it can be seen that the rGO sheets (Fig. 1a) shows a strong absorption peak at 265 nm, which is generally regarded as the excitation of π-plasmon of graphitic structure [33]. Compared with rGO sheets, rGO/ZnO nanohybrids display a new absorption peak at 373 nm, which may be assigned to the intrinsic absorption of ZnO nanocrystals [34]. In addition, with the increase of the loading of ZnO nanocrystals in nanohybrids, the absorption intensity increases sequentially. Fig. 2 shows the FT-IR spectra of GO, rGO and rGO/ZnO nanohybrids (sample Sd). The broad absorptions at about 3425 and 1630 cm^{-1} are assigned to the hydroxyl groups of absorbed H_2O molecules, the peaks around 2970 and 2900 cm^{-1} can be assigned to the asymmetric and symmetric vibrations of C—H, respectively. The absorption band at 1085 cm^{-1} can be assigned to the stretching vibration of C—O. The C=O vibration band at 1724 cm^{-1} (Fig. 2a) disappears after Fe reduction of exfoliated GO (Fig. 2b), indicating that the reduction of GO to rGO is complete [11,35,36]. In addition, the strong absorption band in the range of 430–520 cm^{-1} (Fig. 2c) is corresponding to the vibrations of Zn—O bonds [11,35].

The XRD patterns of the as-prepared rGO sheets prepared via Fe reduction of exfoliated GO for 6 h and rGO/ZnO nanohybrids obtained with the different concentration of zinc salt via a rapid

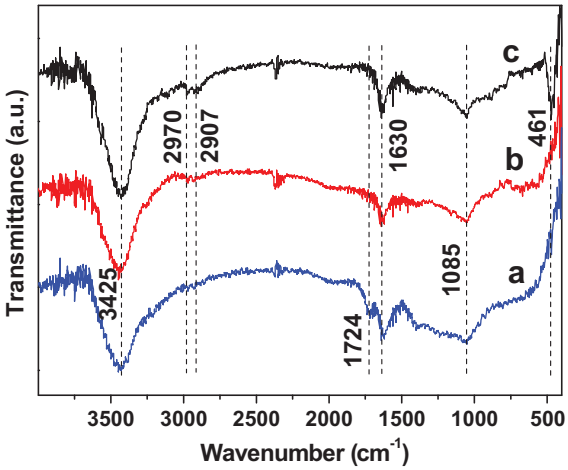

Fig. 2. FT-IR spectra of the as-prepared (a) GO, (b) rGO and (c) rGO/ZnO nanohybrids.

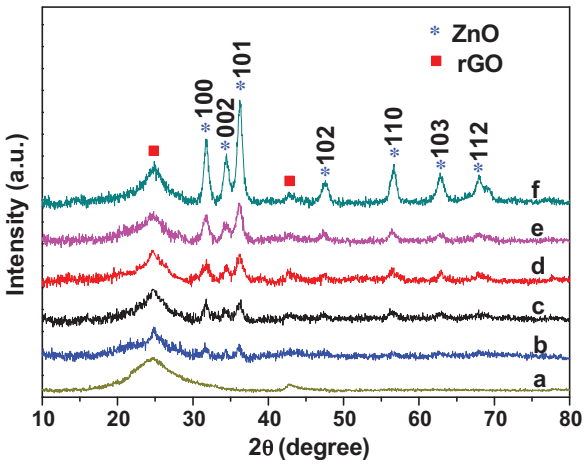

Fig. 3. XRD patterns of the as-prepared (a) rGO sheets and rGO/ZnO nanohybrids obtained via microwave irradiation with different concentration of Zn^{2+}: (b) 0.0023 M, (c) 0.0046 M, (d) 0.0069 M, (e) 0.0092 M, and (f) 0.0115 M.

microwave-assisted method are shown in Fig. 3, and XRD pattern of the GO is shown in Fig. S1 (see supporting information). Patterns b, c, d, e and f belong to the as-prepared rGO/ZnO nanohybrids with the different concentration of zinc salt. The patterns obviously consist of two sets of diffraction peaks (rGO and ZnO), the diffraction peaks marked by square correspond to rGO sheets and the diffraction peaks marked by asterisk correspond to wurtzite phase of ZnO, which is consistent with the standard XRD data file of ZnO (JCPDS standard card no. 79-2205). With the increase of Zn^{2+} concentration, the diffraction intensity of ZnO crystal plane becomes strong gradually, which indicates that the ZnO nanocrystals grow larger and larger. In addition, the average size of ZnO nanocrystals as the concentration of Zn^{2+} increase, calculated using the Debye–Scherrer equation based on the full width at half-maximum of the diffraction peak, are 10.7, 11.2, 12.0, 12.9 and 13.8 nm, respectively (see Table 1).

The typical SEM images of the as-prepared rGO sheets and rGO/ZnO nanohybrids with different concentration of Zn^{2+} are shown in Fig. 4. After the reduction of GO for 6 h, SEM image (Fig. 4a) reveals that the reduced GO material consists of corrugated and crumpled sheets. Corrugation and scrolling are part of the intrinsic nature of rGO sheets, due to the 2D membrane structure becoming thermodynamically stable by bending [37]. From Fig. 4b–f, it is clearly observed that the well-dispersed ZnO nanocrystals are anchored onto the wrinkly rGO sheets, which display a good combination between rGO sheet and ZnO nanocrystals in DEG media via a rapid microwave irradiation process. With increasing concentration of Zn^{2+}, the size and loading of ZnO nanocrystals on the surface of rGO sheets became larger and more, and this result is in a good agreement with that of XRD. Additionally, we have further used an atomic absorption spectrometer to determine the quantitative weight fraction of ZnO nanocrystals in each sample. The results show that the weight fraction of ZnO nanocrystals in the sample increases with increasing Zn^{2+} concentration. More specifically, it is 11.55%, 16.49%, 20.75%, 22.49% and 26.89%, in samples Sb, Sc, Sd, Se and Sf, respectively (see Table 1).

Further morphology and structure characterizations of the as-prepared rGO/ZnO nanohybrids are shown in Fig. 5. Fig. 5a–c is the TEM images of rGO/ZnO nanohybrids obtained with the different concentration of Zn^{2+} (0.0023, 0.0069 and 0.0115 M), which clearly show that well-dispersed ZnO nanocrystals anchored onto rGO sheets uniformly. It can be seen that the ZnO nanocrystals becomes larger and more with the increasing concentration of Zn^{2+},

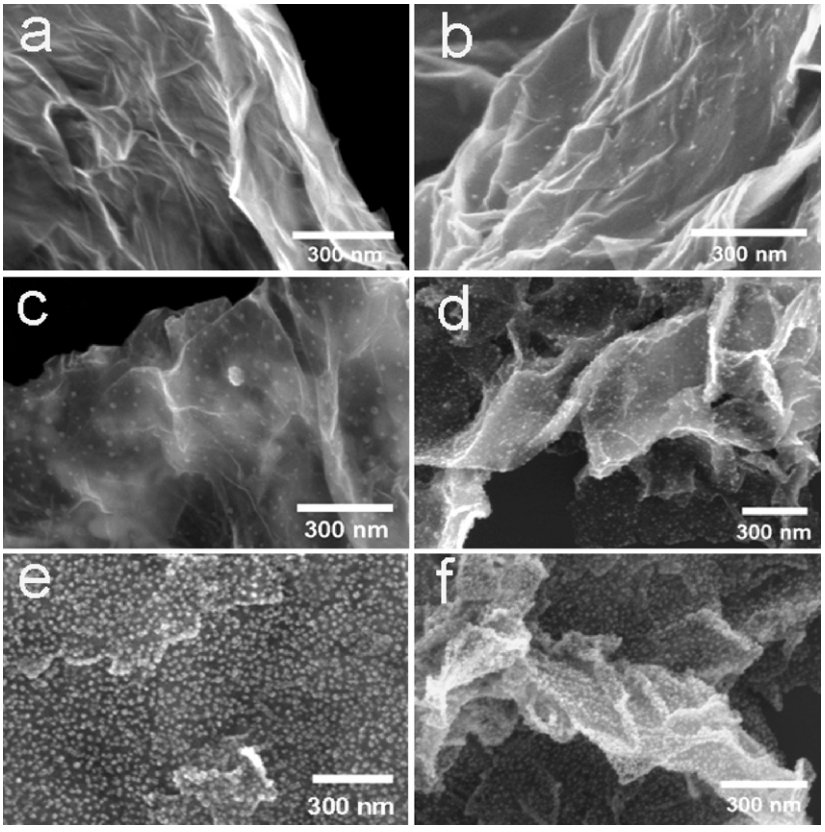

Fig. 4. Typical SEM images of as-prepared (a) rGO sheets and rGO/ZnO nanohybrids obtained with different concentration of Zn^{2+}: (b) 0.0023 M, (c) 0.0046 M, (d) 0.0069 M, (e) 0.0092 M, and (f) 0.0115 M.

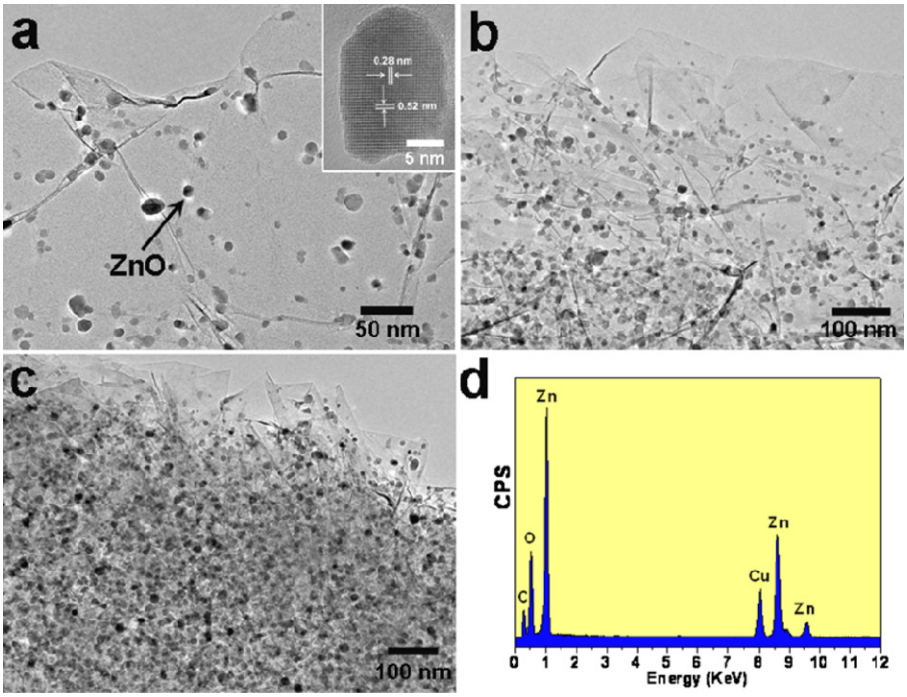

Fig. 5. Typical TEM images of as-prepared rGO/ZnO nanohybrids obtained with different concentration of Zn^{2+}: (a) 0.0023 M, (b) 0.0069 M and (c) 0.0115 M, (d) EDS pattern of the rGO/ZnO nanohybrids.

and this result is also consistent with that of XRD. Interestingly, wrinkled and corner regions of rGO sheets seem to have more ZnO nanocrystals, due to higher density of carboxylic, hydroxyl and epoxy groups [38]. The HRTEM image (inset in Fig. 5a) clearly reveals the anchored ZnO nanocrystal is composed of a small single-crystal plate with about 10 nm in diameter. The EDS pattern of surface layer of as-prepared rGO/ZnO nanohybrids is shown in Fig. 5d, which further confirms the existence of ZnO nanocrystals on the surface of rGO sheets. Additionally, the XRD pattern (Fig. S2) and TEM image (Fig. S3) of pure ZnO obtained via a microwave-assisted non-aqueous route without adding rGO show the size distribution of ZnO spheres is wide (from 100 nm to 1 μm). Thus, the introduction of rGO will help to prevent the aggregation of ZnO nanocrystals.

The structural changes of the as-prepared GO (see Fig. S4), rGO sheets and rGO/ZnO nanohybrids obtained with the different concentration of Zn^{2+} are investigated by the Raman spectroscopy (in Fig. 6), which is a suitable technique to study the ordered/disordered crystal structures of graphite and rGO materials. The usual characteristics of carbon materials in Raman spectra are the G band (~1580 cm^{-1}), which is generally assigned to the E_{2g} phonon of sp^2 bonds of carbon atoms, and the D band (~1350 cm^{-1}) as a breathing mode of κ-point phonons of A_{1g} symmetry, which is attributed to local defects and disorders located at the edges of graphene and graphite platelets [39]. From Fig. 6, two peaks at about 1574 cm^{-1} and 1322 cm^{-1} are observed in the spectra, which are the G and D bands of the as-prepared rGO sheets. After Fe reduction of GO, the ratio of the D to G band intensity (I_D/I_G) increases from 0.89 to 1.91. This result may be attributed to the restoration of numerous graphitic domains from amorphous regions of GO, which gives rise to stronger D band signal [40,41]. The increasing I_D/I_G ratio was usually observed after the chemical reduction of GO into rGO [42,43]. The I_D/I_G for rGO sheets and the rGO/ZnO nanohybrids with increasing concentration of Zn^{2+} are 1.91, 1.88, 1.48, 1.39, 1.11 and 0.92, respectively (see Table 1). The decrease in the I_D/I_G ratio for the rGO/ZnO nanohybrids indicates that a decrease in the average size of the sp^2 domains of C atoms took place during the growth of ZnO nanocrystals [11,19].

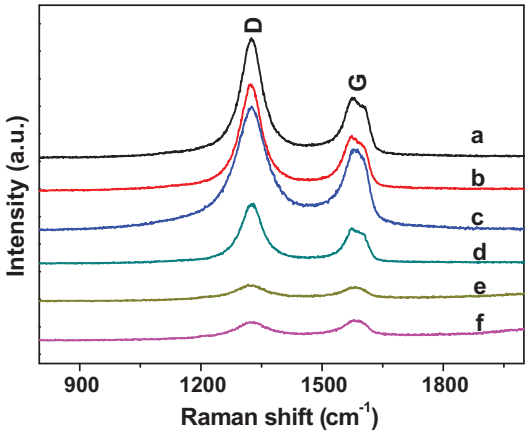

Fig. 6. Raman spectra of (a) rGO sheets and rGO/ZnO nanohybrids obtained with different concentration of Zn^{2+}: (b) 0.0023 M, (c) 0.0046 M, (d) 0.0069 M, (e) 0.0092 M, and (f) 0.0115 M.

The photocatalytic activities of the as-prepared rGO/ZnO nanohybrids were evaluated by the decolorization of the photosensitized dyes including RhB and MB in water. To confirm the enhancement of photocatalytic activity, we use commercial TiO_2 nanoparticles (P25) as a benchmark photocatalyst. Fig. 7 displays time profiles of C/C_0 under visible-light illumination using different photocatalysts, where C is the concentration of dyes after different light irradiation times and C_0 is the initial concentration of dyes before dark adsorption. From Fig. 7a, it shows RhB is very stable under visible light irradiation without the presence of a sample. When different samples were added, the decolorization of RhB to follow the sequences commercial ZnO < rGO < P25 < Sf < Se < Sb < Sc < Sd, which demonstrate all rGO/ZnO nanohybrids possess improved visible-light photocatalytic activity than that of the commercial ZnO nanoparticles and P25. In addition, it also reveals that the photocatalytic activity of the as-prepared rGO/ZnO nanohybrids do not improve monotonously

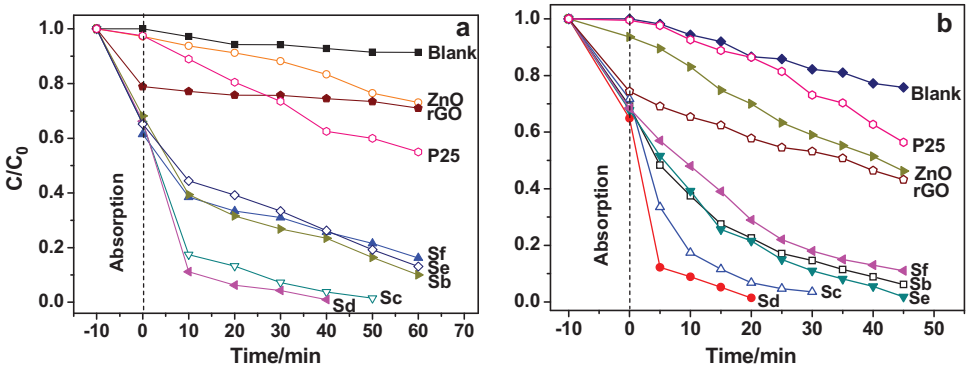

Fig. 7. Photodecolorization of (a) RhB and (b) MB under visible-light illumination by blank, commercial ZnO, P25, rGO and different rGO/ZnO nanohybrids obtained with the different Zn^{2+} concentration.

with the increase of Zn^{2+} concentration. It can be seen that when the concentration of Zn^{2+} is less than 0.0069 M, the photocatalytic activity is improved steadily with increasing amount of zinc precursor. However, further increase in concentration of Zn^{2+} (>0.0069 M) results in decreasing photocatalytic activity. Thus, the best synergetic effect between ZnO nanocrystals and rGO sheets in degrading RhB is attained in sample Sd ($M_{Zn^{2+}}$ = 0.0069 M). Additionally, it is seen that about 2.70%, 21.1%, 2.50%, 38.5%, 34.8%, 31.8%, 34.7% and 33.8% of the RhB is adsorbed for ZnO, rGO, P25, sample Sf, Se, Sb, Sc and Sd after stirring for 2 h in the dark, respectively. Fig. 7b shows the photodecolorization behaviors of MB catalyzed by blank, commercial ZnO nanoparticles, rGO sheets, P25 and rGO/ZnO nanohybrids under visible light illumination, which exhibits a similar regularity like degrading RhB.

Though the explanation of photocatalytic activity by the rGO-semiconductor composite is still controversial [44], the prevailing theory is photosensitization mechanism at present [45]. To ensure the decolorization is merely due to the photosensitized dye decolorization, we measure the photocatalytic properties of rGO/ZnO (sample Sd) in the decolorization of benzoic acid under visible light irradiation to verify this viewpoint, and the results are shown in Fig. S5. It can be seen that the decolorization of benzoic acid is negligible in the presence of sample Sd after 2 h visible-light irradiation. It should be noted that benzoic acid had no absorption in the visible-light region. Therefore, the decolorization of dyes is mainly due to the photosensitization process, rather than the excitation of rGO/ZnO nanohybrids. Considering the work function of RhB (−5.45 eV), excited RhB (−3.08 eV), rGO (−4.42 eV) [45] and the conduction bands of ZnO (−4.05 eV) [11] in Fig. S6. The superior photocatalytic activity of the obtained nanocomposites may be ascribed to the following steps: (a) the dye rather than ZnO is excited by visible light to form the excited dye (dye*), (b) dye* can directly inject electrons into the conduction band or through rGO sheets indirect inject electrons into the conduction band of the ZnO semiconductor, forming conduction band electrons (e_{cb}^-), (c) the electron is trapped by surface adsorbed O_2 to generate various reactive oxidative species (ROSs), (d) the $dye^{\bullet+}$ subsequently self degrades or is degraded by ROSs [10,11,46,47].

Thus, the decolorization efficiency greatly depends on the electron transfer between the dye* and the as-prepared nanohybrids. In this hybrid structure, the electrons in the conduction band of ZnO can easily transfer to rGO, which contribute to improve effective electrons separation. Additionally, rGO sheets with very high surface area-to-volume ratios and extremely high specific surface area to enhance the dispersion of ZnO nanocrystals and allow for greater photon absorption on the photocatalytic surface, leading to the higher photodecolorization efficiency [39,48]. However, the much higher denser of ZnO nanocrystals loading may reduce the quantity of the photogenerated charges due to unfavorable morphology and poorer charge transport through the ZnO nanocrystals. This indicates that, in this particular case, the structure of sample Sd should have the ideal structure when the balancing of charge separation and transport is at optimal and hence demonstrate the most favorable photocatalytic activity. Additionally, the efficiency for the decolorization of dyes (RhB and MB) in the presence of different rGO/ZnO nanohybrids without a cutoff filter under Xe lamp illumination was shown in Fig S7, which indicated that the sample Sd was still more efficient than other samples.

Furthermore, the •OH radicals formed in different nanohybrids decolorization reaction could be probed using a method described previously [49,50]. It is known that •OH reacts with TA in basic solution to generate TAOH, which emits a unique fluorescence signal with its peak centered at ca. 426 nm. Fig. 8 shows significant fluorescent signals associated with TAOH were generated upon visible-light irradiation of the different rGO/ZnO nanohybrids suspended in a TA solution for 10 min. It can be seen that when the concentration of Zn^{2+} was less than 0.0069 M (sample Sd), the fluorescence intensity increases with increasing amount of Zn^{2+}. However, further increase in concentration of Zn^{2+} during the microwave synthesis results in decreasing fluorescence intensity. When only RhB in a TA solution, the emission peak of TAOH could also be observed, but it is much weaker than that of in the presence of rGO/ZnO nanohybrids. Furthermore, the most •OH radicals formed using sample Sd in the decolorization process, and this result is in a good agreement with that of decolorization of dyes.

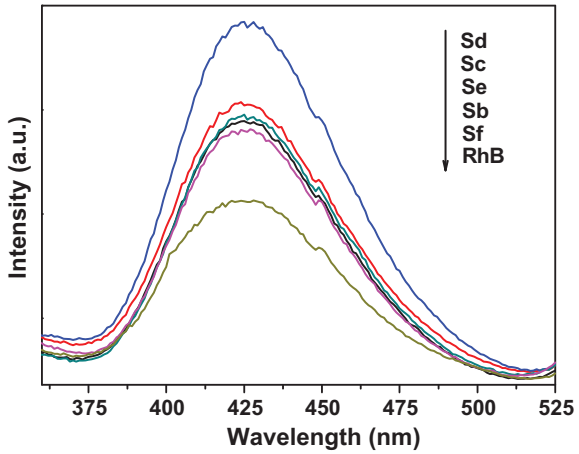

Fig. 8. Fluorescence spectra of TAOH formed by the reaction of TA with •OH radicals generated by different rGO/ZnO nanohybrids under visible-light irradiation for 10 min.

4. Conclusions

In summary, we have developed a novel method for preparing rGO/ZnO nanohybrids in a non-aqueous medium via a rapid microwave irradiation process. The size and loading amount of ZnO nanocrystals anchored is conveniently controlled by varying the concentration of Zn^{2+}. The as-prepared nanohybrids demonstrate well-dispersed ZnO nanocrystals loading and powerful visible-light photocatalytic activity for the decolorization of RhB and MB. The optimal synergistic effect between ZnO and rGO sheets was investigated thoroughly. The enhanced visible-light photocatalytic activity may be attributed to rGO sheets in the composite, which can enhance the specific surface areas of ZnO nanocrystals and electrical transport property from dye* to the rGO semiconductor. This method not only reveals facile synthesis of rGO/ZnO nanohybrids for photocatalytic application, but also can be extended to synthesize other rGO/metal-oxides for different application.

Acknowledgment

Financial supports from the Natural Science Foundation of China (21171146), Zhejiang Provincial Natural Science Foundation of China (Y4110304), and Zhejiang Qianjiang Talent Project (2010R10025) are gratefully acknowledged.

Appendix A. Supplementary data

Supplementary data associated with this article can be found, in the online version, at http://dx.doi.org/10.1016/j.apcatb.2012.06.016.

References

[1] M.R. Hoffmann, S.T. Martin, W.Y. Choi, D.W. Bahnemann, Chemical Reviews 95 (1995) 69–96.
[2] Y. Zhi, Y.G. Li, Q.H. Zhang, H.Z. Wang, Langmuir 26 (2010) 15546–15553.
[3] J.G. Yu, X.X. Yu, Environmental Science and Technology 42 (2008) 4902–4907.
[4] Y. Liu, L. Yu, Y. Hu, C.F. Guo, F.M. Zhang, X.W. Lou, Nanoscale 4 (2012) 183–187.
[5] L.W. Zhang, H.Y. Cheng, R.L. Zong, Y.F. Zhu, Journal of Physical Chemistry C 113 (2009) 2368–2374.
[6] S. Cho, J.W. Jang, J. Kim, J.S. Lee, W. Choi, K.H. Lee, Langmuir 27 (2011) 10243–10250.
[7] S. Anandana, N. Ohashi, M. Miyauchi, Applied Catalysis B: Environmental 100 (2010) 502–509.
[8] R. Ullah, J. Dutta, Journal of Hazardous Materials 156 (2008) 194–200.
[9] Y. Hu, H.H. Qian, Y. Liu, G.H. Du, F.M. Zhang, L.B. Wang, X. Hu, CrystEngComm 133 (2011) 3438–3443.
[10] C.C. Chen, W.H. Ma, J.C. Zhao, Chemical Society Reviews 39 (2010) 4206–4219.
[11] B.J. Li, H.Q. Cao, Journal of Materials Chemistry 21 (2011) 3346–3349.
[12] H.B. Lu, H. Li, L. Liao, J.C. Li, Y. Tian, M. Shuai, M.F. Hu, B.P. Zhu, Nanotechnology 19 (2008) 045605–045611.
[13] G. Yu, J. Gao, J.C. Hummelen, F. Wudl, A.J. Heeger, Science 270 (1995) 1789–1791.
[14] J. Zhong, F. Chen, J.L. Zhang, Journal of Physical Chemistry C 114 (2010) 933–939.
[15] X.H. Xia, Z.J. Jia, Y. Yu, Y. Liang, Z. Wang, L.L. Ma, Carbon 45 (2007) 717–721.
[16] Y. Liu, M.J. Zhou, Y. Hu, H.S. Qian, J.F. Chen, X. Hu, CrystEngComm 14 (2012) 4507–4512.
[17] X. Huang, Z.Y. Yin, S.X. Wu, X.Y. Qi, Q.Y. He, Q.C. Zhang, Q.Y. Yan, F. Boey, H. Zhang, Small 7 (2011) 1876–1902.
[18] S.J. Ding, J.S. Chen, D. Luan, F.Y.C. Boey, S. Madhavi, X.W. Lou, Chemical Communications 47 (2011) 5780–5782.
[19] H.J. Zhang, P.P. Xu, G.D. Du, Z.W. Chen, K. Oh, D.Y. Pan, Z. Jiao, Nano Research 4 (2011) 274–283.
[20] E.P. Gao, W.Z. Wang, M. Shang, J.H. Xu, Physical Chemistry Chemical Physics 13 (2011) 2887–2893.
[21] K.F. Zhou, Y.H. Zhu, X.L. Yang, X. Jiang, C.Z. Li, New Journal of Chemistry 35 (2011) 353–359.
[22] O. Akhavan, ACS Nano 4 (2010) 4174–4180.
[23] Q. Li, B.D. Guo, J.G. Yu, J.R. Ran, B.H. Zhang, H.J. Yan, J.R. Gong, Journal of the American Chemical Society 133 (2011) 10878–10884.
[24] Y. Hu, Y. Liu, H.S. Qian, Z.Q. Li, J.F. Chen, Langmuir 26 (2010) 18570–18575.
[25] Y. Liu, L. Zhou, Y. Hu, C.F. Guo, H.S. Qian, F.M. Zhang, X.W. Lou, Journal of Materials Chemistry 21 (2011) 18359–18364.
[26] M. Baghbanzadeh, L. Carbone, P.D. Cozzoli, C.O. Kappe, Angewandte Chemie International Edition 50 (2011) 2–50.
[27] W.S. Hummers, R.E. Offeman, Journal of the American Chemical Society 80 (1958) 1339.
[28] Z.J. Fan, W. Kai, J. Yan, T. Wei, L.J. Zhi, J. Feng, Y.M. Ren, L.P. Song, F. Wei, ACS Nano 5 (2011) 191–198.
[29] N. Li, G. Liu, C. Zhen, F. Li, L.L. Zhang, H.M. Cheng, Advanced Functional Materials 21 (2011) 1717–1722.
[30] J.H. Lee, D.W. Shin, V.G. Makotchenko, A.S. Nazarov, V.E. Fedorov, J.H. Yoo, S.M. Yu, J.Y. Choi, J.M. Kim, J.B. Yoo, Small 6 (2010) 58–62.
[31] Y. Hu, H.S. Qian, C.F. Guo, T. Mei, CrystEngComm 12 (2010) 2687–2690.
[32] K.F. Lin, H.M. Cheng, H.C. Hsu, L.J. Lin, W.F. Hsieh, Chemical Physics Letters 409 (2005) 208–211.
[33] X. Wang, L.J. Zhi, N. Tsao, J.L. Tomovic, K. Mullen, Angewandte Chemie International Edition 47 (2008) 2990–2992.
[34] D.L. Jin, N. Liao, X.Q. Xu, X.J. Yu, L. Wang, L.C. Wang, Materials Chemistry and Physics 123 (2010) 363–366.
[35] Y. Yang, L.L. Ren, C. Zhang, S. Huang, T.X. Liu, ACS Applied Materials & Interfaces 3 (2011) 2779–2785.
[36] H.L. Guo, X.F. Wang, Q.Y. Qian, F.B. Wang, X.H. Xia, ACS Nano 3 (2009) 2653–2659.
[37] G.X. Wang, X.P. Shen, B. Wang, J. Yao, J. Park, Carbon 47 (2009) 1359–1364.
[38] H.L. Wang, J.T. Robinson, G. Diankov, H. Dai, Journal of the American Chemical Society 132 (2010) 3270–3271.
[39] O. Akhavan, Carbon 49 (2011) 11–18.
[40] X.G. Mei, J.Y. Ouyang, Carbon 49 (2011) 5389–5397.
[41] S. Stankovich, D.A. Dikin, R.D. Piner, K.A. Kohlhaas, A. Kleinhammes, Y. Jia, Y. Wu, S.T. Nguyen, R.S. Ruoff, Carbon 45 (2007) 1558–1565.
[42] C.Y. Su, Y.P. Xu, W.J. Zhang, J.W. Zhao, A.P. Liu, X.H. Tang, C.H. Tsai, Y.Z. Huang, L.J. Li, ACS Nano 4 (2010) 5285–5292.
[43] H.J. Shin, K.K. Kim, A. Benayad, S.M. Yoon, H.K. Park, I.S. Jung, M.H. Jin, H.K. Jeong, J.M. Kim, J.Y. Choi, Y.H. Lee, Advanced Functional Materials 19 (2009) 1987–1992.
[44] Q.J. Xiang, J.G. Yu, M. Jaroniec, Chemical Society Reviews 41 (2012) 782–796.
[45] J.T. Zhang, Z.G. Xiong, X.S. Zhao, Journal of Materials Chemistry 21 (2011) 3634–3640.
[46] Z.G. Xiong, L.L. Zhang, J.Z. Ma, X.S. Zhao, Chemical Communications 46 (2010) 6099–6101.
[47] P.F. Ji, J.L. Zhang, F. Chen, M. Anpo, Applied Catalysis B: Environmental 85 (2009) 148–154.
[48] T.G. Xu, L.W. Zhang, H.Y. Cheng, Y.F. Zhu, Applied Catalysis B: Environmental 101 (2011) 382–387.
[49] J.H. Huang, K.N. Ding, X.C. Wang, X.Z. Fu, Langmuir 25 (2009) 8313–8319.
[50] G. Liu, P. Niu, L.C. Yin, H.M. Cheng, Journal of the American Chemical Society 134 (2012) 9070–9073.